



OPEN

Discovery of a new class of integrin antibodies for fibrosis

Ji Zhang^{1✉}, Tao Wang², Ashmita Saigal¹, Josephine Johnson³, Jennifer Morrisson², Sahba Tabrizifard², Scott A. Hollingsworth⁴, Michael J. Eddins⁴, Wenxian Mao³, Kim O'Neill⁵, Margarita Garcia-Calvo⁵, Ester Carballo-Jane³, DingGang Liu⁶, Taewon Ham⁶, Qiong Zhou⁶, Weifeng Dong⁶, Hsien-Wei Meng², Jacqueline Hicks⁷, Tian-Quan Cai⁸, Taro Akiyama¹, Shirly Pinto¹, Alan C. Cheng⁴, Thomas Greshock⁷, John C. Marquis², Zhao Ren³, Saswata Talukdar¹, Hussam Hisham Shaheen² & Masahisa Handa^{2✉}

Lung fibrosis, or the scarring of the lung, is a devastating disease with huge unmet medical need. There are limited treatment options and its prognosis is worse than most types of cancer. We previously discovered that MK-0429 is an equipotent pan-inhibitor of α v integrins that reduces proteinuria and kidney fibrosis in a preclinical model. In the present study, we further demonstrated that MK-0429 significantly inhibits fibrosis progression in a bleomycin-induced lung injury model. In search of newer integrin inhibitors for fibrosis, we characterized monoclonal antibodies discovered using Adimab's yeast display platform. We identified several potent neutralizing integrin antibodies with unique human and mouse cross-reactivity. Among these, Ab-31 blocked the binding of multiple α v integrins to their ligands with IC50s comparable to those of MK-0429. Furthermore, both MK-0429 and Ab-31 suppressed integrin-mediated cell adhesion and latent TGF β activation. In IPF patient lung fibroblasts, TGF β treatment induced profound α SMA expression in phenotypic imaging assays and Ab-31 demonstrated potent in vitro activity at inhibiting α SMA expression, suggesting that the integrin antibody is able to modulate TGF β action through mechanisms beyond the inhibition of latent TGF β activation. Together, our results highlight the potential to develop newer integrin therapeutics for the treatment of fibrotic lung diseases.

Idiopathic pulmonary fibrosis (IPF) is a chronic, fibrosing interstitial lung disease with unknown etiology. Patients suffer from chronic coughs and deteriorating breathing difficulties. The median survival is 2.5–3.5 years from diagnosis. Despite the severe clinical impact, there are limited treatment options for lung fibrosis. In 2014, the FDA approved the use of Pirfenidone and Nintedanib in IPF patients. Both drugs slow the decline of lung function as measured by the decrease of FVC (forced vital capacity), a surrogate endpoint measurement¹. However, neither drug appears to stop disease progression, relieve breathing difficulty, or substantially improve patient survival. There is an unmet medical need to develop new IPF therapies that bring clinically meaningful efficacy to patients.

In recent years, the integrin family of cell adhesion molecules has emerged as key mediators of tissue fibrosis. Among the 24 known integrin heterodimers, five α v integrins (α v β 1, α v β 3, α v β 5, α v β 6, and α v β 8) transduce mechanical and biochemical signals from fibrotic extracellular matrix into the cell, activate latent TGF β , and subsequently modulate fibroblast adhesion, migration, and growth². The α v integrins primarily interact with the RGD (Arginine-Glycine-Aspartic acid) peptide present in fibronectin and vitronectin (α v β 1, α v β 3, and α v β 5), or with the RGD motif of the TGF β latency-associated peptide (LAP) (α v β 1, α v β 6, and α v β 8)^{2–5}. As a result, α v integrins play a key role in the regulation of TGF β signaling⁶. Dysregulated expression and response to TGF β has been implicated in a wide variety of disease processes including fibrotic disease and chronic inflammation⁷. The epithelium-specific α v β 6 integrin binds to latent TGF β and facilitates release of the mature cytokine, a

¹Departments of Cardiometabolic Diseases, MRL, Merck & Co., Inc., 2000 Galloping Hill Road, Kenilworth, NJ 07033, USA. ²Discovery Biologics, MRL, Merck & Co., Inc., 2000 Galloping Hill Road, Kenilworth, NJ 07033, USA. ³Quantitative Biosciences, MRL, Merck & Co., Inc., 2000 Galloping Hill Road, Kenilworth, NJ 07033, USA. ⁴Computational & Structural Chemistry, MRL, Merck & Co., Inc., 2000 Galloping Hill Road, Kenilworth, NJ 07033, USA. ⁵In Vitro Pharmacology, MRL, Merck & Co., Inc., 2000 Galloping Hill Road, Kenilworth, NJ 07033, USA. ⁶SALAR, MRL, Merck & Co., Inc., 2000 Galloping Hill Road, Kenilworth, NJ 07033, USA. ⁷Discovery Chemistry, MRL, Merck & Co., Inc., 2000 Galloping Hill Road, Kenilworth, NJ 07033, USA. ⁸In Vivo Pharmacology, MRL, Merck & Co., Inc., 2000 Galloping Hill Road, Kenilworth, NJ 07033, USA. ✉email: ji.zhang1@alumni.duke.edu; masahisa.handa@merck.com

process called TGF β activation^{3,8}. Deletion of $\beta 6$ integrin *in mice* is protective against bleomycin-induced lung fibrosis³, and an anti-mouse $\alpha v\beta 6$ antibody has shown similar beneficial effects in preclinical animal studies⁹. An $\alpha v\beta 6$ antibody (BG00011/Biogen) and a small molecule inhibitor GSK3008348 were used in clinical trials of IPF patients (clinicaltrials.gov identifier NCT03573505, NCT03069989)¹⁰. $\alpha v\beta 1$, the less-known member of the integrin family, was recently shown to be highly expressed in activated fibroblasts and modulate lung and liver fibrosis in mice⁵. Additionally, $\alpha v\beta 8$ integrin, another regulator of latent TGF β activation, modulates chemokine secretion and dendritic cell trafficking^{4,11}. $\beta 8$ knockout mice and mice treated with a blocking $\beta 8$ antibody are protected against airway inflammation and fibrosis^{4,12}. Although the role of a pan- αv inhibitor has not been extensively tested in the clinic for lung indications, evidence from multiple lines of work suggest that modulating αv integrin activity will lead to anti-fibrotic effects in various tissues. A report by Henderson et al. demonstrated that depletion of αv integrin in myofibroblasts lead to protection against hepatic fibrosis induced by carbon tetrachloride, renal fibrosis induced by unilateral ureter obstruction, and lung fibrosis induced by bleomycin⁶. Furthermore, a small molecule RGD mimetic CWHM12 similarly attenuates liver and lung fibrosis⁶. The complexity of the integrins and their role in the progression of the disease suggest that a pharmacological inhibitor of multiple integrin subtypes would be required to produce meaningful effects on delaying or inhibiting the progression of fibrosis. Interestingly, recent genome-wide association analysis of 400,102 individuals identifies an association of reduced αv gene expression with increased lung function¹³.

Historically, MSD has contributed significantly to the development of integrin therapeutics by bringing forth the first approved small molecule inhibitor Aggrastat (Tirofiban) for acute coronary artery syndrome^{14,15}. We also developed a small molecule integrin inhibitor MK-0429 with good oral bioavailability in humans¹⁶. MK-0429 was initially designed as an RGD mimetic against $\alpha v\beta 3$ integrin that incorporates key pharmacophores representing the guanidine and carboxylic acid of the RGD tripeptide sequence^{17,18}. We recently found that MK-0429 is an equipotent pan-inhibitor of multiple αv integrins, and it reduces proteinuria and renal fibrosis in an experimental diabetic nephropathy model¹⁹. In the present work, we further demonstrate that MK-0429 significantly inhibits fibrosis progression in a bleomycin-induced lung fibrosis mouse model. We also identified several potent αv integrin antibodies with unique human and mouse cross-species affinity. Among these, Ab-31 demonstrated potent *in vitro* activity at inhibiting TGF β -induced α SMA expression in lung fibroblasts derived from IPF patients than did MK-0429 and another benchmarking molecule. Taken together, our work has provided further experimental validation of targeting αv integrin for the treatment of fibrotic lung diseases.

Results

αv integrin expression in fibrotic lungs. Recent studies suggested pharmacological targeting of αv integrins is beneficial in multiple tissue fibrosis, including lung, liver, and kidney fibrosis⁶. To explore the potential role for integrin antagonist in the lung, we first examined the expression of αv integrins in normal human lung fibroblasts (NHLF), normal human bronchial epithelial cells (NHBE), small airway epithelial cells (SAEC), bronchial smooth muscle cells (BSMC), pulmonary artery smooth muscle cells (PASMC), and pulmonary artery endothelial cells (PAEC). The cells were treated with or without TGF β , a master regulator of myofibroblast activation and extracellular matrix deposition⁷. The total pool of αv integrins were immunoprecipitated from the cell lysates and subsequently blotted for the abundance of each β subunit. The expression $\alpha v\beta 6$ integrin was highly restricted to epithelial cells NHBE and SAEC (Fig. 1A). $\alpha v\beta 6$ is a known epithelium-specific integrin and it binds to latent TGF β in the extracellular matrix, subsequently inducing local activation of the growth factor and promoting fibrosis^{3,20}. Meanwhile, $\alpha v\beta 3$ and $\alpha v\beta 5$ were more broadly expressed in a variety of lung cell types (Fig. 1A). $\alpha v\beta 1$, the less-known member of the integrin family, was barely detected in lung fibroblasts (NHLF) and appeared more abundant in epithelial cells (NHBE) and smooth muscle cells (BSMC) upon TGF β treatment (Fig. 1A), suggesting that $\alpha v\beta 1$ is a highly inducible integrin expressed in multiple cell types. This observation is consistent with our previous report in kidney cell types¹⁹, pointing to a potential role for $\alpha v\beta 1$ integrin beyond fibroblasts.

Bleomycin-induced lung fibrosis has been commonly used to evaluate the efficacy of a therapeutic agent in preclinical animal studies. After the initial phase of inflammation and cytokine storm, animals develop fibrosis and progressive lung function decline²¹. To develop the bleomycin model in mice, we administered various doses of bleomycin via intra-tracheal instillation (Fig. 1B). Twenty days after dosing, lungs were collected for histological evaluation. Bleomycin induced a dose-dependent increase of fibrosis in the lung, as shown by the overall modified Ashcroft score, α SMA-positive cells, and collagen deposition (Picosirius red staining) (Fig. 1B). More cells were reactive to CD68 upon bleomycin administration, indicating significant inflammatory macrophage infiltration. Fibrosis and inflammation were evident across all lung lobes evaluated, suggesting widespread lesions in the lung (Supplemental Fig. S1A,B).

To determine the expression of αv integrins in bleomycin-injured lungs, we next carried out Sally Sue simple western analysis of total lung extracts by using a capillary-based electrophoresis system²². The abundance of αv and $\beta 5$ integrins was significantly upregulated in bleomycin-treated animals, comparing to those from the saline-treated group (Fig. 1C). $\beta 3$ integrin expression appeared to be slightly reduced; whereas, $\beta 6$ and $\alpha 5$ integrin expression was variable among individual animals. Additionally, phospho-Tyr397 and total FAK levels were increased in the bleomycin-treated group, suggesting activation of classical integrin signaling in the lung and providing additional experimental support for αv integrin targeting in this model.

MK-0429 suppresses fibrosis progression in bleomycin model. We previously found that MK-0429 is an equipotent pan-inhibitor of αv integrins which reduces proteinuria and renal fibrosis in diabetic nephropathy model¹⁹. We next determined whether MK-0429 could inhibit the progression of lung fibrosis *in vivo*. Five days after bleomycin administration, we treated mice with MK-0429 (200mpk via osmotic minipump) or a

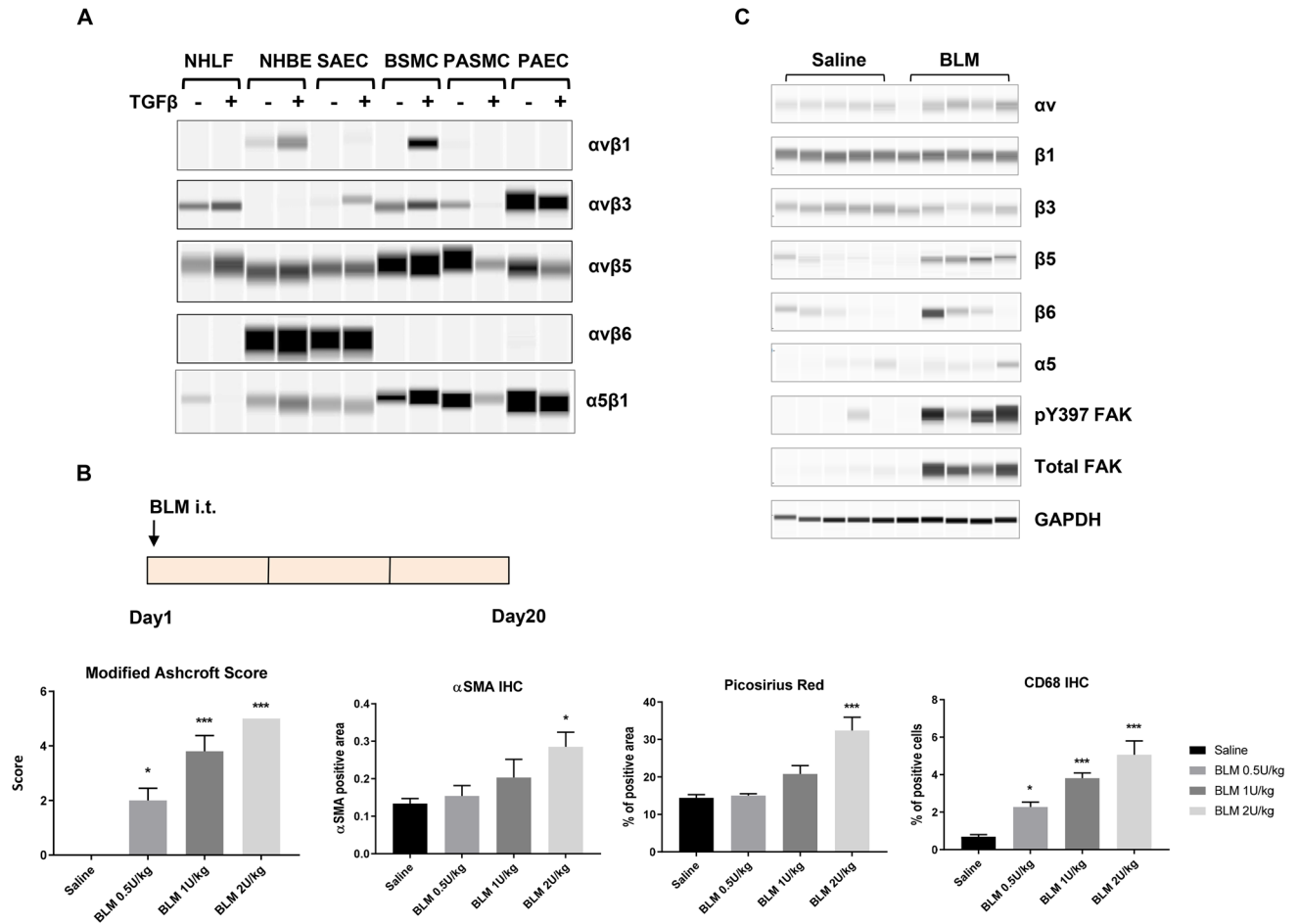


Figure 1. Changes of αv integrin expression upon fibrosis induction in the lung. **(A)** The expression of αv integrins in various human primary lung cell types upon $TGF\beta$ (5 ng/ml for 24 h) treatment. Following immunoprecipitation with an anti- αv antibody, the $\alpha v\beta 1$, $\alpha v\beta 3$, $\alpha v\beta 5$, and $\alpha v\beta 6$ heterodimers were detected by Sally Sue simple western analysis after using antibodies that recognize each individual β -subunit. Normal human lung fibroblast, NHLF; normal human bronchial epithelial cells, NHBE; small airway epithelial cells, SAEC; bronchial smooth muscle cells, BSMC; pulmonary artery smooth muscle cells, PASM; pulmonary artery endothelial cells, PAEC. Full-length blot images are presented in Supplemental Fig. S6A–E. **(B)** Development of a bleomycin-induced lung fibrosis model in mice. Bleomycin (BLM) was administered at the indicated doses via intra-tracheal (i.t.) instillation. After 20 days, lungs were collected for histological analyses. Modified Ashcroft score, Picosirius red staining, immunohistochemical analyses of α SMA and CD68 of total lung were quantified and shown (mean \pm SEM, $n = 5$). Immunohistochemistry, IHC. One-way ANOVA followed by Tukey’s test, * $p < 0.05$, ** $p < 0.01$, *** $p < 0.005$ vs Saline group. **(C)** Integrin expression and signaling in fibrotic lungs (BLM 0.5U/kg bw) was determined by Sally Sue simple western analysis using antibodies that recognized the individual α or β -subunits. Each lane represents total lung homogenate for one animal, $n = 5$ for saline or BLM group. GAPDH level in total lung lysates was used as a loading control. Full-length blot images are presented in Supplemental Fig. S6F–N.

benchmarking agent (Nintedanib, 60mpk, po, qd). The animals were analyzed for histology and biomarkers after treatment for 14 days (Fig. 2A). This treatment regimen allowed us to probe the efficacy of the integrin mechanism after bypassing the initial phase of inflammation and cytokine storm.

Plasma concentration levels of MK-0429 and Nintedanib were determined at 2 h after the last dose at the end of the study. The mean plasma concentration was 3701 ± 902 ng/ml for MK-0429, and 656 ± 229 ng/ml Nintedanib (Fig. 2B), consistent with the previous report¹⁹. Notably, this concentration of Nintedanib exceeds the level of no-observed-adverse-effect-level (NOAEL) dose identified in mice from Nintedanib’s pharmacology review (Ref 2058320Orig1s000).

Bleomycin instillation significantly decreased the bodyweight when compared to mice treated with Saline (Supplemental Fig. S2A,B). After MK-0429 and Nintedanib administration, there was no significant body weight difference between the bleomycin group and different treatment groups. There was no significant difference for percentage change of body weight among various groups. Mouse lungs were collected at Day 19 for histological evaluation. As shown by the Masson Trichrome staining (Fig. 2C), control lung tissues had normal lung structure with some collagen around the bronchioles (panels a and d). Administration of bleomycin caused severe

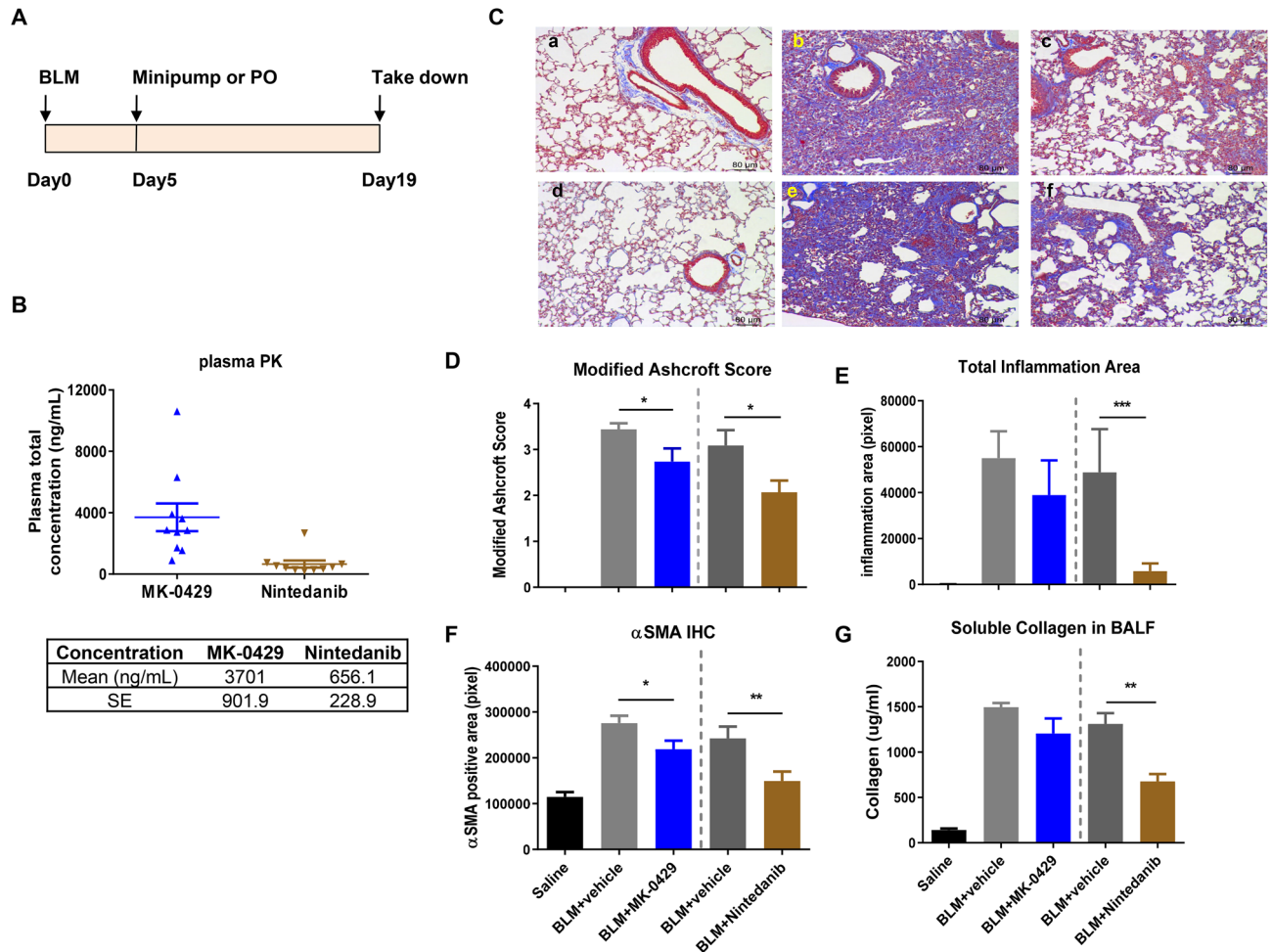


Figure 2. MK-0429 inhibits lung fibrosis in the bleomycin mouse model. (A) Schematics of compound administration in BLM model. 5 days after BLM intra-tracheal instillation, the animals were given MK-0429 (200 mpk via osmotic minipump for 2 weeks) or Nintedanib (60 mpk po qd for 2 weeks). Lungs were collected at Day 19 for histological and biochemical evaluation. mpk, milligrams per kilogram body weight; po, *Per os*, oral administration; qd, *Quaque die*, every day. (B) Plasma total drug concentration was measured 2 h after final oral dose at Day 19. (C) Representative Masson Trichrome staining of mouse lungs. a and d, saline intra-tracheal instillation; b-f, BLM intra-tracheal instillation; a and d, no compound treatment; b, vehicle in minipump; c, MK-0429 in minipump; e, vehicle po; f, Nintedanib po. (D) Modified Ashcroft scores of mouse lung. Mean \pm SEM, n = 10. One-way ANOVA followed by Tukey's test, * $p < 0.05$, ** $p < 0.01$, *** $p < 0.005$ vs BLM-vehicle group. (E) Total inflammation area in mouse lungs. Mean \pm SEM, n = 10. One-way ANOVA followed by Tukey's test, * $p < 0.05$, ** $p < 0.01$, *** $p < 0.005$ vs BLM-vehicle group. (F) Immunohistochemical analysis of α SMA. Mean \pm SEM, n = 10. One-way ANOVA followed by Tukey's test, * $p < 0.05$, ** $p < 0.01$, *** $p < 0.005$ vs BLM-vehicle group. (G) Soluble collagen content in bronchoalveolar lavage fluid (BALF). Mean \pm SEM, n = 10. * $p < 0.05$, ** $p < 0.01$, *** $p < 0.005$ vs BLM-vehicle group.

multifocal and diffuse fibrosis, thickening of alveolar septa, intra-alveolar fibrosis, and increased perivascular and peribronchiolar infiltration of inflammatory cells (Fig. 2C, panel b). Nintedanib significantly improved modified Ashcroft score and decreased inflammation after 14 days treatment (Fig. 2C, panel c; Fig. 2D,E). Meanwhile, MK-0429 treatment at 200mpk significantly decreased the modified Ashcroft score and led to a nonstatistical significant decrease of inflammation in the lung (Fig. 2D,E). Myofibroblast proliferation in lung tissue was detected by α SMA IHC staining. As shown in Fig. 2F, bleomycin significantly increased the immunoreactivity for α SMA, both Nintedanib and MK-0429 significantly decreased bleomycin-induced α SMA expression.

Bronchioalveolar lavage fluid (BALF) was also collected for biomarker analyses. Bleomycin increased soluble collagen content and TIMP-1 levels in BALF (Fig. 2G, Supplemental Fig. S2C). Nintedanib significantly decreased BALF soluble collagen and TIMP-1 content after 14 days treatment. The decreases in BALF soluble collagen and TIMP-1 content upon MK-0429 treatment did not reach statistical significance. Together, our results demonstrate that MK-0429 is effective at reducing fibrosis progression in a bleomycin lung injury model.

Discovery of novel α v integrin monoclonal antibodies with human and mouse cross-reactivity. To obtain new integrin inhibitors for fibrosis, we utilized Adimab yeast surface display platform to screen

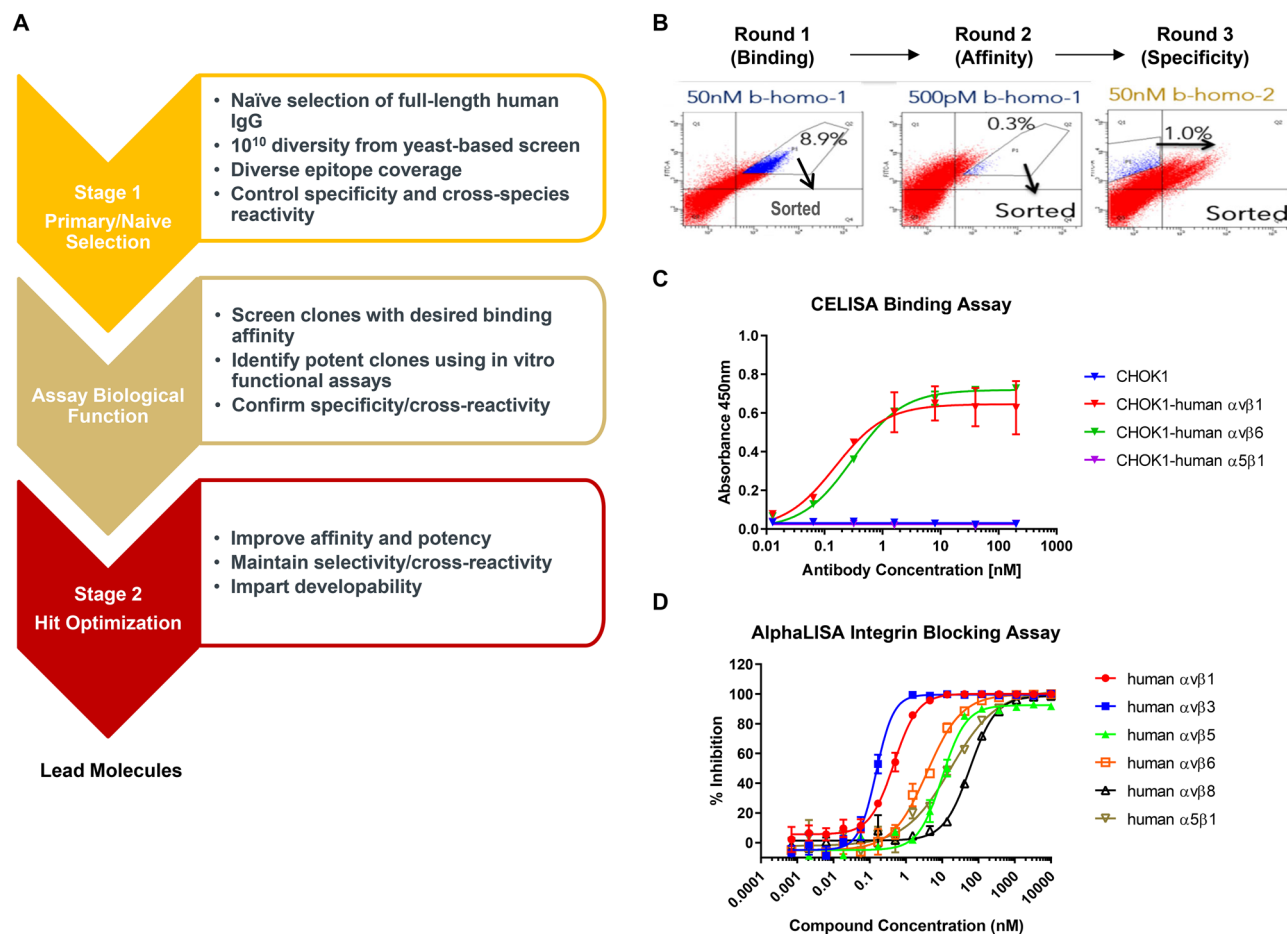


Figure 3. Integrin antibody screening and assay development. **(A)** Staged efforts to screen integrin antibodies from human naïve IgG library by using Adimab's yeast display platform. **(B)** IgG-expressing yeast clone selection process. The X-axis represents integrin binding and the Y-axis reflects antibody expression. Yeast cell population with strong antigen binding (boxed) was sorted out for the next round of selection. **(C)** Cell-based ELISA (CELISA) binding assays were used as the primary screen for integrin antibody selection. Dose-dependent binding of the benchmarking integrin antibody mAb-24 to various integrin-expressing CHOK1 cells was shown. **(D)** AlphaLISA integrin-ligand binding assays were used for in vitro functional screen. Dose-dependent inhibition of human integrin-ligand binding by MK-0429 in AlphaLISA assay panel.

for tool molecules with better potency than MK-0429. A full-length human naïve IgG library was used for the identification and counter selection of αv -integrin antibodies (Fig. 3A). Extracellular domains of recombinant human and mouse $\alpha v \beta 1$, $\alpha v \beta 3$, $\alpha v \beta 5$, $\alpha v \beta 6$, $\alpha v \beta 8$, and $\alpha 5 \beta 1$ integrin proteins (Supplemental Table S1) were purified, biotinylated, and used as baits to screen for specific binders through several rounds of enrichment by magnetic bead isolation or fluorescence activated cell sorting (FACS). In round 1 and 2, IgG-presenting yeast clones were enriched for target binding and affinity using bait $\alpha v \beta x$ proteins at a concentration of 50 nM and 500 pM, respectively (Fig. 3B). Yeast cell population with strong antigen binding was sorted out for the next round of selection. In round 3, the best-binders were depleted for $\alpha 5 \beta 1$ binding and PSR (poly-specificity reagent) non-specific binding. From the initial screen, we identified 188 unique binders for IgG expression, purification, and functional characterization.

To examine the binding affinity of each clone, we next generated a set of CHOK1 cell lines that stably expressed human or mouse $\alpha v \beta 1$, $\alpha v \beta 3$, $\alpha v \beta 5$, $\alpha v \beta 6$, $\alpha v \beta 8$, and $\alpha 5 \beta 1$ integrins. The relative abundance of each integrin was determined by FACS analyses after staining the cells with corresponding integrin antibodies (Supplemental Fig. S3, Supplemental Table S2). The binding affinity and specificity of each yeast clone to CHOK1 parental cells or CHOK1- $\alpha v \beta 1$, $\alpha v \beta 6$, or $\alpha 5 \beta 1$ -expressing cells were determined upon antibody titration in a cell-based ELISA (CELISA) assay. As shown in Fig. 3C, a benchmarking monoclonal antibody mAb-24 preferentially bound to human $\alpha v \beta 1$ and $\alpha v \beta 6$ integrin but not $\alpha 5 \beta 1$ integrin in this high-throughput cell-based binding assay. 34 antibody clones with tenfold higher binding affinity towards $\alpha v \beta 1$ and $\alpha v \beta 6$ integrins were selected for further functional characterization.

We previously determined the in vitro potency and selectivity of MK-0429 by using solid-phase ELISA and thermal shift assays¹⁹. To develop a more sensitive and high-throughput functional assay to screen integrin antibodies, we utilized the AlphaLISA platform to determine the blocking of integrins-ligand binding by antibodies. It has been shown that fibronectin, vitronectin, and TGF β latency-associated peptide (LAP) function as

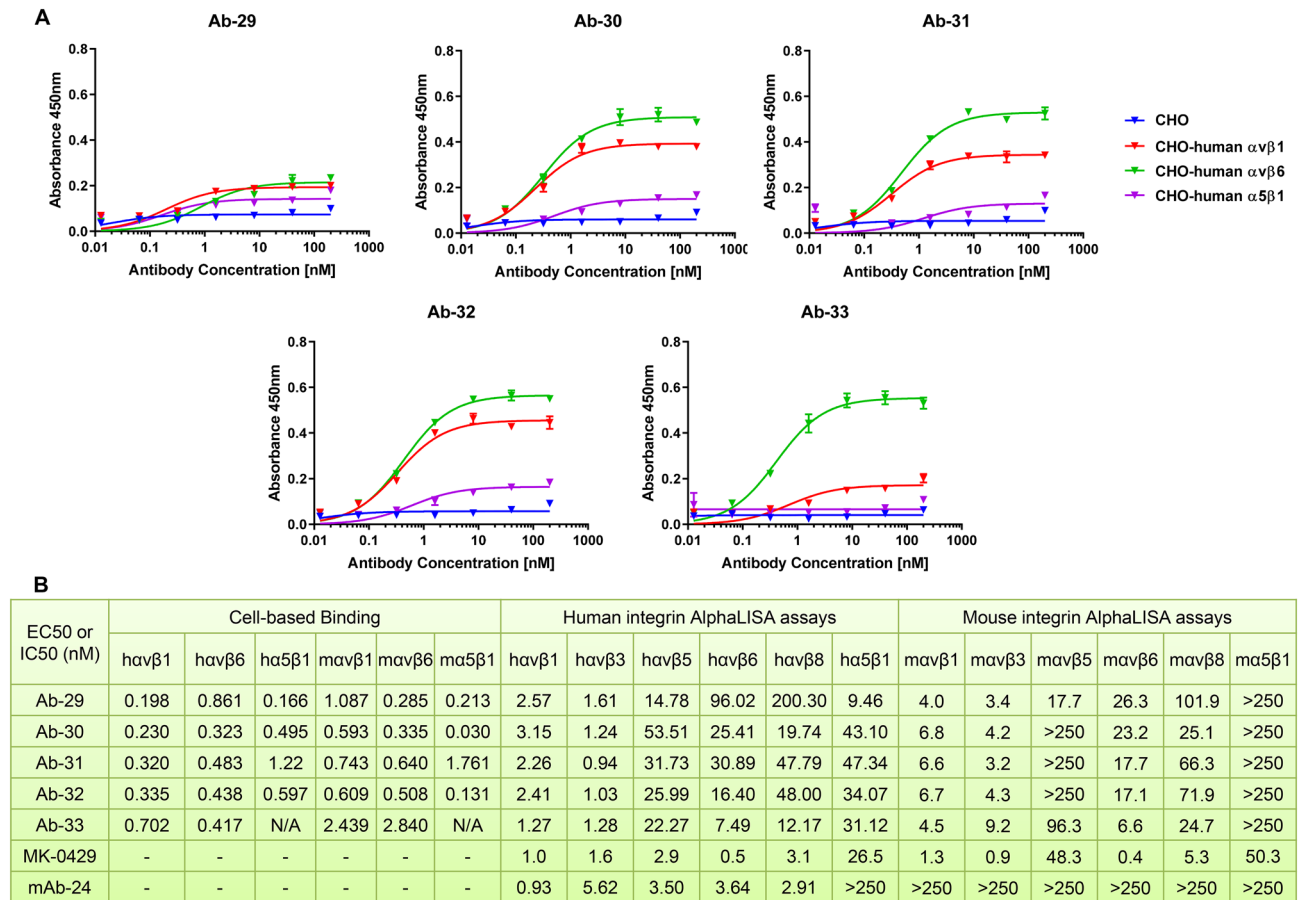


Figure 4. Discovery a set of antibodies with strong blocking activities against both human and mouse αv integrins. **(A)** Titration of Ab-29, Ab-30, Ab-31, Ab-32, and Ab-33 for their binding to CHOK1-human $\alpha v\beta 1$, $\alpha v\beta 6$, and $\alpha 5\beta 1$ stable cell lines in CELISA assays. **(B)** EC50 of Ab-29, Ab-30, Ab-31, Ab-32, and Ab-33 in CELISA assays, as well as their IC50 in human and mouse AlphaLISA integrin blocking assays.

endogenous ligands for $\alpha v\beta 1$, $\alpha v\beta 3/5$, and $\alpha v\beta 6/8$ ^{5,23–25}. Additionally, $\alpha 5\beta 1$ is a well-known fibronectin receptor²⁶. Thus, we used different ligands for each integrin (Supplemental Table S3) and optimized the assay conditions to obtain curve-fitted IC50 values for MK-0429. As shown by the results in Fig. 3D, MK-0429 demonstrated potent inhibition against human $\alpha v\beta 1$ (IC50 = 0.46 nM), $\alpha v\beta 3$ (IC50 = 0.15 nM), $\alpha v\beta 5$ (IC50 = 9.9 nM), $\alpha v\beta 6$ (IC50 = 3.8 nM), $\alpha v\beta 8$ (IC50 = 58.3 nM), and $\alpha 5\beta 1$ (IC50 = 17.3 nM), consistent with our previous solid-phase ELISA assay results¹⁹. Subsequently, we selected strong binders to examine their abilities to block integrin function in both human and mouse AlphaLISA assays.

Our initial screen led to the identification of 5 unique antibody clones from different germlines that potently inhibited multiple αv -integrins. The top clones were selected for light chain shuffling and affinity maturation on heavy chain CDR1 and CDR2 sequences. Daughter clones with improved binding affinity and potency were expressed in mammalian cells and purified for further characterization to identify lead molecules (Fig. 3A).

After an initial screening and two rounds of affinity maturation, we identified 5 unique antibodies, Ab-29, Ab-30, Ab-31, Ab-32, and Ab-33, which strongly bound to human $\alpha v\beta 1$ and $\alpha v\beta 6$ integrins, and in a lesser extent towards $\alpha 5\beta 1$ integrin (Fig. 4A). Their EC50s of cell-based binding towards each integrin are shown in Fig. 4B, suggesting that they are pan- αv inhibitors. Notably, those five molecules were also reactive to mouse $\alpha v\beta 1$, $\alpha v\beta 6$, and $\alpha 5\beta 1$ integrins (Fig. 4B, Supplemental Fig. S4A). To date, there are no αv -integrin antibodies with human and mouse cross-reactivity reported. We next carried out AlphaLISA integrin blocking assays to examine the effect of each antibody on integrin-ligand binding. As shown in Fig. 4B, Ab-29, Ab-30, Ab-31, Ab-32, and Ab-33 substantially inhibited human $\alpha v\beta 1$, $\alpha v\beta 3$, $\alpha v\beta 5$, $\alpha v\beta 6$, $\alpha v\beta 8$, and $\alpha 5\beta 1$ integrins, with IC50s comparable to those of MK-0429 and the benchmarking mAb-24. MK-0429 was potent at blocking mouse integrin-ligand binding in all cases except mouse $\alpha v\beta 6$ and $\alpha 5\beta 1$, where it showed weaker activities (Fig. 4B, Supplemental Fig. S4B). Ab-29, Ab-30, Ab-31, Ab-32, and Ab-33 also strongly inhibited mouse $\alpha v\beta 1$, $\alpha v\beta 3$, $\alpha v\beta 6$, and $\alpha v\beta 8$ integrins. Their activities towards mouse $\alpha 5\beta 1$ integrin were negligible. The binding affinity (Kd) of each antibody to selected integrin proteins was within the range of 2–48 nM as assessed by the ForteBio Octet Red system (Supplemental Fig. S4C). Epitope binning revealed unique binding sites of our antibodies compared to other known αv -integrin antibodies (data not shown). Overall, our molecules represent a new class of αv -integrin blocking antibodies that could be used as mouse surrogates for rodent preclinical studies.

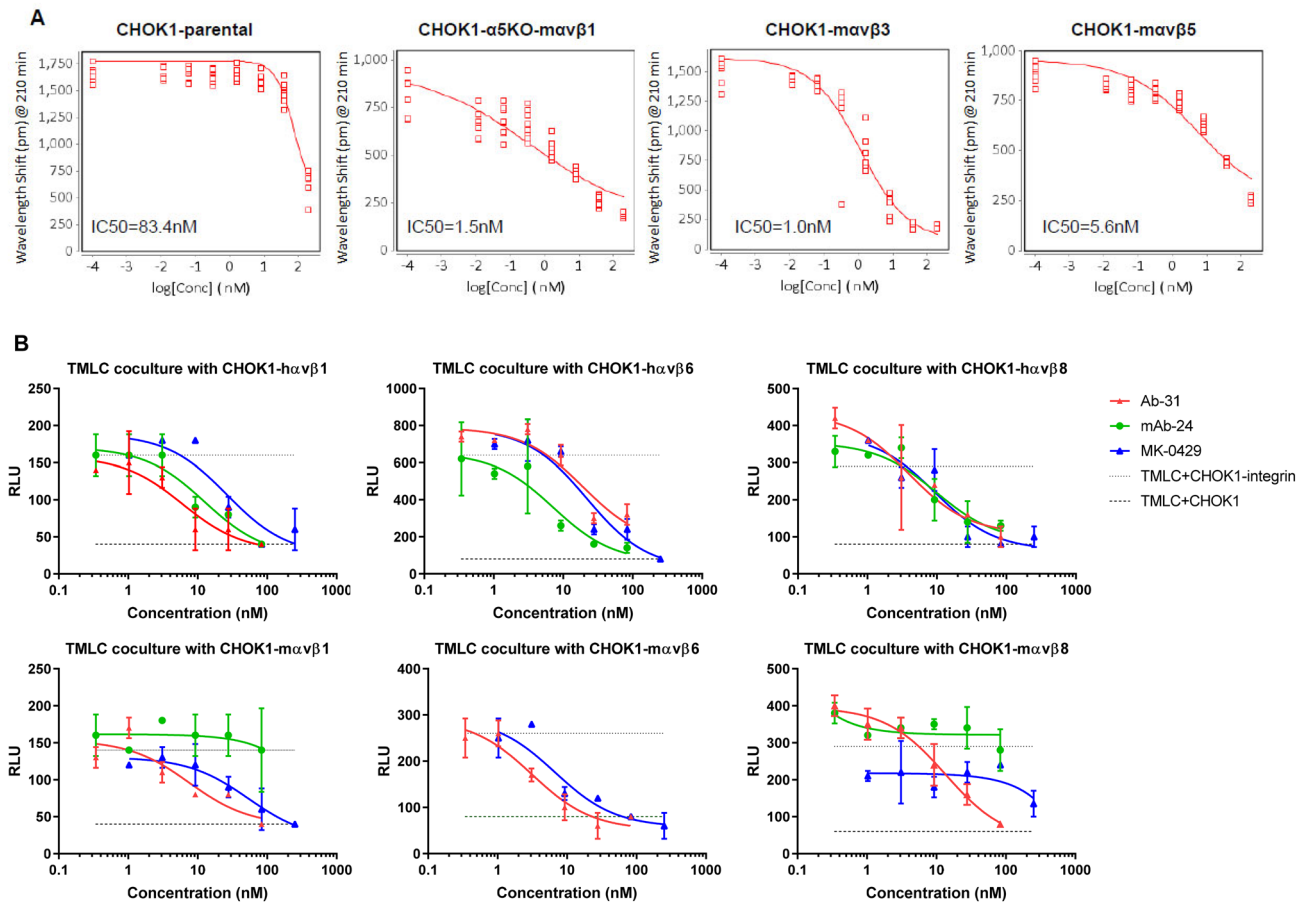


Figure 5. Ab-31 inhibits integrin-mediated cell adhesion and latent TGF β activation. **(A)** The effect of Ab-31 on the adhesion of CHOK1 parental, CHOK1- α 5KO-mav β 1, CHOK1-mav β 3, and CHOK1-mav β 5 cells to fibronectin or vitronectin matrix. **(B)** pan- α v integrin inhibitors suppress latent TGF β activation in the transfected Mink lung epithelial cells (TMLC) and CHOK1-integrin co-culture system. The effects of Ab-31, MK-0429, and benchmarking mAb-24 on PAI-1 luciferase activity were shown.

Ab-31 blocks integrin-mediated cell adhesion. Previous studies utilized cell adhesion assays to determine integrin subtype selectivity and cellular function^{5,27}. The cell-based assay measures the binding of ligand to integrins that are endogenously present or over-expressed on the cell surface. Compared to in vitro functional assays using recombinant protein, cell adhesion results are more reflective of native integrin-ligand binding conformation. We generated CHOK1 stable cell lines that expressed various human and mouse α v β x integrins (Supplemental Fig. S3). Both α v β 1 and α 5 β 1 can function as fibronectin receptors in cell adhesion assay^{26,28}. To delineate the role of α v β 1 in cell adhesion, we deleted endogenous hamster α 5 gene in CHOK1 cells via CRISPR knockout/KO technology, and subsequently overexpressed α v β 1 to generate a CHOK1- α 5KO- α v β 1 stable line. We next examined the effect of MK-0429 and our top monoclonal antibody clone, Ab-31, on the adhesion of cells to fibronectin or vitronectin matrix. MK-0429 showed little inhibitory activity in CHOK1 parental cells on fibronectin; however, it potently reduced the adhesion of mouse α v β 1-expressing CHOK1- α 5KO cells (Supplemental Fig. S5A). Cell adhesion of mouse α v β 3 and α v β 5 on a vitronectin matrix were also decreased upon MK-0429 treatment. Similarly, Ab-31 significantly inhibited mouse α v β 1, α v β 3, and α v β 5 integrin-mediated cell adhesion, with IC₅₀s of 1.5 nM, 1.0 nM, and 5.6 nM respectively (Fig. 5A). The cell-based assays showed that Ab-31 is a potent α v-integrin inhibitor in a setting that resembles native integrin conformation.

Ab-31 substantially inhibits integrin-mediated latent TGF β activation. The epithelium-specific α v β 6 integrin blocks the activation of latent TGF β ^{3,8}, a major mechanism-of-action for α v-integrin to modulate fibrosis. Rifkin et al. transfected mink lung epithelial cells with a firefly luciferase reporter under the control of PAI-1 (plasminogen activator inhibitor-1) promoter²⁹. The transcription of PAI-1 is tightly controlled by the TGF β -Smad pathway^{30,31}. When co-culturing these transfected mink lung epithelial cells (TMLC) with another cell type-expressing integrin, the luciferase activity is driven by the abundance of mature TGF β presented in extracellular matrix and culture medium. This co-culturing system provides a sensitive measurement of latent TGF β activation by integrins.

In addition to α v β 6 integrin, both α v β 1 and α v β 8 have been shown activating latent TGF β ^{5,11,32}. We next examined the activity of our monoclonal antibody Ab-31 against TGF β activation in the TMLC-integrin co-culture

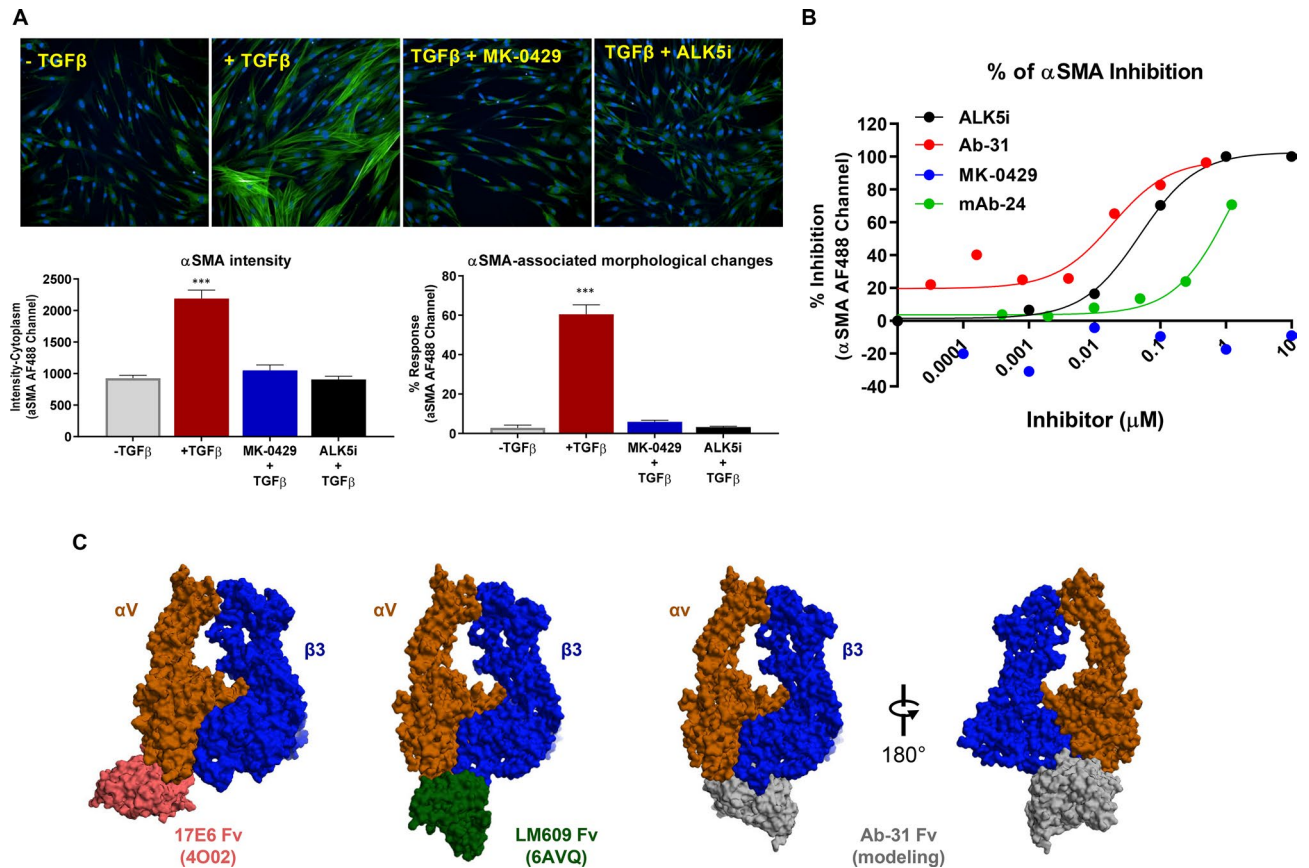


Figure 6. Ab-31 reduces TGFβ-induced αSMA expression in lung fibroblasts. (A) Normal human lung fibroblasts were stimulated with TGFβ (5 ng/mL) and stained with anti-αSMA antibody for immunofluorescence analysis. Cells were pre-treated with or without MK-0429 (10 μM) or the ALK5 inhibitor SB-525334 (10 μM) 30 min before the addition of TGFβ. 48 h after the treatment, cells were imaged with Opera Phenix high-content screening system for αSMA expression (fluorescence intensity) and αSMA-associated morphological changes (STAR program). (B) The effects of Ab-31, MK-0429, and benchmarking antibody mAb-24 on TGFβ-associated αSMA induction in IPF patient lung fibroblasts. (C) Structural modeling predicts a distinct integrin binding mode for Ab-31. The structures of two therapeutic monoclonal antibodies, Abituzumab (17E6, RCSB PDB: 4O02) and LM609 (RCSB PDB: 6AVQ), in complex with αvβ3 integrin were shown to highlight the difference in binding modes for each molecule. A model of Ab-31 and αvβ3 integrin complex was determined by docking of related antibody sequence to αvβ3 structure (see “Methods”). For visualization, only the Fv region of each antibody were shown.

system. Notably, Ab-31 substantially blocked the activation of latent TGFβ by human and mouse αvβ1, αvβ6, and αvβ8 integrins, with IC₅₀ at 6.1 nM, 19.1 nM, 3.9 nM, 7.5 nM, 3.1 nM, and 13.5 nM, respectively (Fig. 5B). MK-0429 also demonstrated strong inhibitory effect at TGFβ activation except in a mouse αvβ8 co-culture assay. The benchmarking antibody, mAb-24, was potent in human αvβ1, αvβ6, and αvβ8 co-culture systems, but elicited minimal activity against mouse integrins, which is consistent with its activities in AlphaLISA assays. Together, our results found that pan-αv integrin monoclonal antibody Ab-31 strongly inhibits integrin-mediated cellular functions, including cell adhesion and latent TGFβ activation.

Ab-31 demonstrates potent inhibitory activity against TGFβ-induced αSMA expression. In addition to the inhibition of latent TGFβ activation, αv-integrin inhibitors also function downstream of TGFβ signaling^{19,33}. To further characterize the activities of our molecules in a fibrosis-relevant cell type, we next examined the expression of αSMA in primary human lung fibroblasts. Normal human lung fibroblasts were cultured, treated with TGFβ, and stained for αSMA by high-content phenotypic imaging analysis (Fig. 6A). Upon TGFβ induction, the fluorescence intensity of αSMA was vastly increased (Fig. 6A), and αSMA-associated cellular morphological changes were recognized as stimulated cells by the machine learning-based STAR software (Harmony high-content imaging and analysis software, PerkinElmer Inc.). Pretreating cells with MK-0429 or with SB-525334, a potent inhibitor of TGFβ type I receptor ALK5 (activin receptor-like kinase)³⁴ significantly reduced αSMA intensity and the percentage of stimulated cells following TGFβ treatment.

After establishing this αSMA phenotypic assay platform, we next examined the effects of integrin inhibitors on lung fibroblasts derived from IPF patients. As seen in the healthy human fibroblast assays, the expression of αSMA and percentage of stimulated cells among fibroblasts from IPF patients were also increased after TGFβ treatment (Fig. 6B). The ALK5 inhibitor, SB-525334, potently inhibited TGFβ-mediated αSMA induction in

patient fibroblasts, with IC₅₀ of 56 ± 22 nM. Notably, MK-0429 had minimal activity inhibiting αSMA induction even at a concentration of 10 μM, suggesting that the network for αSMA regulation is distinct in IPF patient fibroblasts than that of normal human lung fibroblasts. The benchmarking monoclonal antibody mAb-24 was also less effective at inhibiting αSMA expression with IC₅₀ above 1 μM. Interestingly, Ab-31 demonstrated a strong dose-dependent inhibition of αSMA intensity and associated morphological changes with IC₅₀ of 33 ± 21 nM, similar to that of the ALK5 inhibitor (Fig. 6B). It is noteworthy that Ab-31 was ineffective in normal human lung fibroblasts (data not shown), raising a possibility that this molecule preferentially recognizes integrin confirmation under fibrotic state. Our data demonstrate that Ab-31 was a potent inhibitor of TGFβ signaling in IPF patient lung fibroblasts and exhibits strong anti-fibrotic activity in cell-based assays.

Structural modeling of integrin-antibody complex. Over the past 20 years, a diverse set of integrin monoclonal antibodies have been discovered and extensively characterized that can elicit inhibitory, stimulatory, or neutral activity upon integrin binding³⁵. Integrin antibodies are also known to recognize active conformational epitope, such as 12G10 and 9EG7 clones of β1-integrin antibodies^{36–38}. To further understand the mechanism of action of our antibody, we next set out to predict how it interacts with integrins.

The first crystal structure of integrin heterodimer was solved in 2001 and revealed a bent inactive confirmation of αvβ3 integrin ectodomains³⁹. Since then, several integrin-antibody complex structures have been determined and have provided valuable information in regard to their regulatory function. 17E6 (Abituzumab) is a therapeutic pan-αv integrin antibody that has been tested in multiple Phase 2 clinical trials in cancer patients and systemic sclerosis patients with interstitial lung disease⁴⁰ (clinicaltrials.gov identifier NCT02745145). The crystal structure of the 17E6 Fab fragment in complex with αvβ3 revealed that the antibody exclusively bound to the αv subunit and helped to establish a potential allosteric inhibition mechanism via steric hindrance (PDB: 4O02)⁴¹. As illustrated in the left panel of Fig. 6C, the variable region (Fv) of 17E6 binds to an epitope outside the ligand binding interface of the α- and β-subunits. In contrast, LM609 is an αvβ3-specific blocking antibody of which the humanized variants, Vitaxin and Etaracizumab (Abeigrin), have been tested in several clinical trials for oncology indications^{42–44}. A combination of crystallographic and cryo-EM work from Borst et al. found that LM609 bound to the apex of the integrin headpiece close to but without directly obstructing the RGD-binding site⁴⁵. The structure of LM609 Fv fragment in complex with αvβ3 integrin is illustrated in the second left panel of Fig. 6C, with an epitope locating at the interface between the α- and β-subunits. Compared to either of these characterized antibodies, Ab-31, as well as other top clones from our screen, represented a unique class of pan-αv integrin antibodies with human and mouse cross-reactivity. To better understand the mechanism of integrin inhibition by Ab-31, we set out to model the Ab-31-integrin complex through homology modeling and docking. Using the antibody Fv sequence, we generated a series of 10 models for the Fv structure of Ab-31 using MOE (Chemical Computing Group). The lowest energy structure was then docked against the known structure of the known αvβ3 structure (see “Methods”). Following visualization and filtering of potential poses against known experimental variants, the final pose shown in Fig. 6C was determined. Interestingly, the model predicted that Ab-31 bound directly at the interface between α- and β-subunits and somewhat blocked access to the RGD-ligand binding site (Fig. 6C, right panels), indicating a distinct mode of action compared to 17E6 and LM609. This model is consistent with our epitope binning findings that Ab-31 had an epitope that did not overlap with other integrin antibodies (data not shown). Further structural and biophysical characterization will help to better understand its mode of action and cross reactivity.

Discussion

IPF is multi-factorial disease and the dominant mechanism that drives pathogenesis is unclear. The mechanism of action for Pirfenidone is presently unknown, likely involving multiple pathways that include anti-inflammation and TGFβ suppression⁴⁶. Nintedanib is an inhibitor for multiple receptor tyrosine kinases, such as VEGFR, PDGFR, and FGFR⁴⁷. Currently, there are several mechanisms being tested in the clinic for IPF patients, including but not limited to the CTGF antibody Pamrevlumab, the Autotaxin inhibitor GLPG-1690, and recombinant Pentraxin 2 (PRM-151). In recent years, integrin inhibitors have emerged as key mediators of tissue fibrosis. In particular, αv-containing integrins, such as αvβ6, modulate local TGFβ activation and myofibroblast activation with strong preclinical validation for lung fibrosis^{3,9,48}. In the present study, we used MK-0429 as a tool molecule to further validate the role of αv integrins in preclinical lung fibrosis model. Furthermore, we initiated an antibody discovery campaign and discovered a set of novel integrin monoclonal antibodies with human and mouse cross-reactivity. Among these, Ab-31 potently blocked integrin-ligand binding, inhibited integrin-mediated cell adhesion, suppressed both the activation of latent TGFβ and the αSMA expression induced by activated TGFβ. Notably, Ab-31 demonstrated potent activity at inhibiting TGFβ response in IPF patient lung fibroblasts, making it a unique tool molecule to study anti-fibrotic efficacy in vivo. It is intriguing that both Ab-31 and MK-0429 have comparable activities when tested in vitro using AlphaLISA integrin-ligand blocking assays, but their impact on TGFβ signaling in IPF patient lung fibroblasts was drastically different. In previous reports, bivalent 17E6 and LM609 were postulated to interfere with integrin clustering and internalization on the cell surface, enhancing their therapeutic effects over that of a monovalent Fab fragment^{41,45}. It is possible that Ab-31 also functions by regulating integrin clustering and internalization. Further structural and biophysical characterization is warranted to elucidate the inhibitory mechanism of Ab-31.

The complexity of integrin biology and the overlapping roles of multiple integrins in the progression of the disease suggest that a pharmacological pan inhibitor would be beneficial, leading to clinically meaningful inhibition of fibrosis. Interestingly, a recent GWAS study of large population provides strong genetic evidence that supports targeting the αv integrin to improve lung function, potentially expanding the use of αv integrin inhibitors to a broader patient population, such as chronic obstructive pulmonary disease (COPD)¹³. The

poly-pharmacology nature of an α v inhibitor raises potential safety concerns. Notably, MK-0429 has been tested in the clinic in osteoporosis patients over the duration of 52 weeks with relatively well-tolerated safety profile^{16,49}. One main mechanism-of-action of integrin inhibitors is to inhibit latent TGF β activation. Compared to the preclinical cardiovascular safety signal observed with TGF β receptor inhibition, the safety profile of pan- α v integrin inhibition is more tolerable. Recently, an α v β 6 antibody (BG00011) was withdrawn from phase 2 clinical trials in IPF patients due to safety concerns (clinicaltrials.gov identifier NCT03573505). It will be of interest to compare the efficacy and safety profiles of α v β 6-specific and pan- α v inhibitors. The preferential effect of Ab-31 on IPF patient lung fibroblasts over normal human lung fibroblasts suggested that this antibody may selectively recognize either an active or diseased-associated integrin conformational state, making it an interesting molecule with a potential improved therapeutic index.

In summary, our present work describes the discovery a new class of integrin monoclonal antibodies that potentially inhibit integrin-ligand binding, integrin-mediated cell adhesion, and TGF β signaling. Our molecules exhibit distinct human and mouse cross-reactivity and structural modeling predicts a unique mode of inhibition. Future computer-aided rational design will allow the development of optimized molecules for new anti-fibrotic therapies.

Methods

Cultured cells and reagents. Normal human lung fibroblasts (Lonza) and Primary Human IPF Lung Parenchymal Fibroblasts (Donor2) (BioIVT, #PCR-70-0214) were incubated at 37 °C and 5% CO₂. To induce fibrotic response in primary cells, a final concentration of 5 ng/ml of recombinant human TGF β 1 (BioLegend, #580702) was added to the culture media and treated for 24–48 h. Anti-TGF β neutralizing antibody (1D11) and the isotype control mouse IgG1 were from BioXcell. SB-525334 and bleomycin were from Sigma. MK-0429 was synthesized by Merck & Co., Inc., Kenilworth, NJ, USA. CHOK1-integrin stable lines were cultured in DMEM/F12, Glutamax (Gibco #10565018), 10% FBS (Gibco 310091148), 1 \times Pen/Strep (Gibco 315140-148), and 6 μ g/mL Puromycin (Gibco #A1113803).

Recombinant integrin proteins. The full extracellular domains for all α and β integrin subunits (human and mouse versions, Supplemental Table S1) were codon optimized for mammalian expression (Genewiz, NJ) and inserted into the HindIII and XhoI sites of pcDNA3.1. α v and α 5 contained a C-terminal (GGGS)₃ linker with an acidic coiled-coil with a cysteine for disulfide-bond formation, a GG-Avitag (Avidity, CO), and a hexahistidine tag. β 1, β 3, β 5, β 6, and β 8 contained a C-terminal (GGGS)₃ linker with a basic coiled-coil with a cysteine, and a GG-Avitag. For expression, 10 L of Expi293 cells (ThermoFisher, standard protocol) were co-transfected with 0.5 mg/L each of both an α and a β subunit, either human (h) or mouse (m) and grown for 72 h at 37 °C in shake flasks (hav β 1, hav β 3, hav β 5, hav β 6, hav β 8, ha5 β 1, mav β 1, mav β 3, mav β 5, mav β 6, mav β 8, ma5 β 1). Media was harvested by centrifugation and soluble supernatant concentrated to 1 L by TFF (tangential flow filtration, Pellicon 10 K) in 25 mM Tris pH 8.0, 300 mM NaCl, 40 mM Imidazole. Sample was centrifuged again (15 min @ 3500 g) prior to purification. For expression, the sample was loaded over a HisTrap FF (2 \times 5 mL) column pre-equilibrated in 25 mM Tris pH 8.0, 300 mM NaCl, 40 mM Imidazole, washed for 15 CV with the equilibration buffer, and eluted with a gradient from 40 to 500 mM Imidazole (in 25 mM Tris pH 8.0, 300 mM NaCl). Protein not needing biotinylation was further purified using a Superdex 200 column in 25 mM TRIS pH 8.0, 150 mM NaCl, 1 mM MgCl₂, 1 mM CaCl₂. Eluted fractions were concentrated to 2 mg/mL, aliquoted and frozen. For biotinylation, sample that needed to be biotinylated after elution from the initial HisTrap FF column was concentrated to 3.0 mg/mL and desalted/buffer exchanged (ZebaSpin desalting column) into 25 mM Tris pH 8.0, 150 mM NaCl. Sample was combined with Biomix B and BirA (as per Avidity protocol) and incubated at 4 °C for 14 h. Biotinylated sample was further purified using a Superdex 200 column in 25 mM TRIS pH 8.0, 150 mM NaCl, 1 mM MgCl₂, 1 mM CaCl₂. Eluted fractions were concentrated to 2 mg/mL, aliquoted and frozen. Biotinylation was verified by either streptavidin binding gel shift, or with the Pierce Fluorescence Biotin Quantification Kit (#46610).

Antibody discovery, optimization, and production. De novo antibody discovery for α v-integrins were executed on pre-immune Adimab yeast display libraries with a diversity of 10¹⁰⁵⁰. The soluble proteins used in the yeast display selections are biotinylated recombinant integrin ectodomain proteins described in Supplemental Table S1. All proteins were analytically and biophysically verified by binding against known integrin antibodies (Supplemental Table S2), SEC, SDS-PAGE, and endotoxin analyses. Briefly, a yeast IgG library was subjected to multiple rounds of selection by magnetic activated cell sorting (MACS) and fluorescence activated cell sorting (FACS, BD ARIA III) in PBS buffer containing 1 mM MnCl₂. Selections were performed using 100 nM human or mouse α v β 1 followed by rounds of enrichment for populations that were cross-reactive to 100 nM of α v β 3, α v β 5, α v β 6, and α v β 8. Along with the selection progress, the decreased antigen concentrations are also applied to enhance selection pressure to identify higher affinity binders. Isoform-specific selections were achieved by negative sorting of α 5 β 1 to collect the population that are not binding to α 5 β 1. Top clones were isolated by affinity maturing its parental clone through shuffling the light chain and optimizing heavy chain CDR1 and CDR2 sequences. The selection of optimization libraries was repeated using 10 nM α v β 1 followed by enrichment for cross-reactivity to α v β 3, α v β 5, α v β 6, and α v β 8, but not α 5 β 1. The isolated clones were then sequenced to identify the unique antibodies and screened for isoform binding profiles by Octet Red. The heavy chain and light chain genes of top clones were cloned into pTT5 mouse Fc-mutated IgG1 backbone vector and produced in Chinese Hamster Ovary (CHO) cells and purified using protein A chromatography. Antibodies were formulated at 2 mg/mL in a buffer composed of 20 mM sodium acetate and 9% sucrose (pH 5.5). Isotype control antibodies was used in subsequent assays.

Integrin cell-based ELISA (CELISA) assay. Cell binding EC₅₀ data for antibodies were obtained for CHOK1 parental cells and CHOK1 cells expressing human or mouse $\alpha\beta 1$, $\alpha\beta 6$, and $\alpha 5\beta 1$ integrins by cell-based ELISA. Three days prior to the assay cells were seeded at 10,000 cells per well in 100 μL /well of media in Falcon 96-well Flat-Bottom Tissue Culture Plates (REF 353916), resulting in an even cell monolayer in each well on the day of the assay. On the day of the assay, media was removed from the cells and a fivefold titration of primary antibodies was added at concentrations ranging from 0 to 200 nM in TBSF + MnCl_2 buffer (25 mM Tris, 0.15 M NaCl, 0.1% BSA, 0.5 mM MnCl_2 , pH 7.5). Cells incubated with primary antibody solution for 1 h at room temperature. Primary antibody was removed and plates were washed twice with 150 μL /well of $1 \times \text{DPBS} + \text{Tween}20$ (TEKnova Cat # P0297, diluted to $1 \times$ in distilled water GIBCO #15230-147), before adding 50 μL /well of a 1:5000 dilution of HRP-conjugated goat anti-mouse IgG (Southern Biotech, #1030-05) in TBSF + MnCl_2 . After 30 min of incubation at room temperature, secondary antibody was removed, and cells were washed twice with 150 μL /well of $1 \times \text{DPBS} + \text{Tween}20$. 50 μL /well of TMB substrate (1-Step Ultra TMB-ELISA, Thermo Scientific, #34028) was added, incubated with cells at room temperature and 50 μL /well of TMB stop solution (Seracare, #KPL 50-85-05) was added after 5 min. Absorbance was read on a TECAN plate reader at 450 nm, with a 620 nm reference wavelength.

Integrin AlphaLISA assay. In the AlphaLISA integrin assays, we used a HEPES based buffer (25 mM HEPES pH 7.4, 137 mM NaCl, 1 mM MgCl_2 , 1 mM MnCl_2 , 2 mM CaCl_2 , 2.7 mM KCl, and 0.05% Tween-20). Optimal assay conditions were determined with a titration of the reagents for signal noise ratio (S/N), linear range, etc. For the respective integrins, we used the final concentrations described in Supplemental Table S3. Briefly, the testing antibody (8 μL) was added as a 4x (of final testing concentration) solution in the HEPES buffer described previously into a 384w AlphaPlate (Perkin Elmer #6005350). Then the integrin and ligand were added sequentially as 8x (4 μL each). Plates were sealed and incubated at room temperature for 2 h. Then $4 \times$ acceptor bead solution (8 μL) was added, and the plates were resealed and incubated at RT for 1 h. Finally, $4 \times$ (8 μL) donor beads solution was added in a darkened room and incubated for 45 min at room temperature. Plates were read on the Envision (Perkin Elmer) in AlphaScreen mode within 3 h of donor bead addition.

Cell adhesion assay. For plate preparation, Epic 384-well assay plates (Corning #5040) were washed with OptiMEM (Gibco #31985-070) and coated with murine fibronectin (Abcam #ab92784) at a concentration of 0.1 μg /well for CHO- $\alpha 5\text{KO-mav}\beta 1$ cells; murine vitronectin (Abcam #ab92727) at 0.075 μg /well for CHO- $\text{mav}\beta 3$ cells; or murine vitronectin at 0.125 μg /well for CHO- $\text{mav}\beta 5$ (all at a volume of 25 μL /well in OptiMEM), for 1 h. Coating solution was then removed by flicking and plates were washed with OptiMEM and blocked with 25 μL /well of assay buffer [1% Ovalbumin (Sigma #A5503-10G) in OptiMEM containing 1X Pen-Strep (Gibco #15140-148)]. A 5-min baseline reading was taken on a Corning Epic Plate Reader (Model: Epic BT-157900) before removing the assay buffer and adding cells pre-incubated with inhibitors. The Epic plate reader detects cellular mass redistribution (adhesion) on the plate surface as a picometer wavelength shift over time. For inhibitor titration preparation: fivefold serial dilutions of small molecule inhibitor MK-0429 or antibody inhibitor Ab-31 were prepared in assay buffer at 4X the final concentration in a 384-well polypropylene plate in a volume of 15 μL per well, starting at a concentration of 800 nM. For cell preparation: On the day of the assay, frozen cell stocks were thawed and transferred to 10 mL complete media (DMEM/F12 + Glutamax (Gibco #10565-018) containing 10% FBS (Gibco #10091-148) and 1X Pen-Strep (Gibco 315140-148) for CHO and CHO- $\text{mav}\beta 3$ cells, or F12K Nutrient Mixture (Gibco #21127-022) containing 10% FBS (Gibco #10091-148) and 1X Pen-Strep (Gibco #15140-148) for CHO- $\alpha 5\text{KO-mav}\beta 1$ and CHO- $\text{mav}\beta 3$ cells at 37 °C in a 15 mL falcon tube. Cells were pelleted, re-suspended in 10 mL of complete media and allowed to recover for 1.5 h at 37 °C with gentle shaking. Following cell recovery step, cells were counted using Trypan blue and re-suspended to densities between 2^6 and 2.67^6 cells/mL in assay buffer. 45 μL /well of this cell solution was added to the plate containing 15 μL /per well of inhibitor using an Agilent Bravo liquid handler. Final cell concentrations were between 1.5^6 and 2^6 cells/mL and final inhibitor concentrations were in a range from 0 to 200 nM. Cells were incubated with the inhibitors for 1 h at RT with gentle rocking, after which 50 μL per well was transferred to the Epic assay plate, and a time course of cell adhesion was monitored for an additional 3 h.

Latent TGF β activation assay. Transfected mink lung epithelial cell (TMLE) cell line containing the TGF β responsive PAI-1 promoter driving luciferase expression²⁹ and the CHO-K1 human and mouse $\alpha\beta x$ integrin cell lines were grown under optimized growth conditions to 90% confluency. TMLE cells were trypsinized and plated at 25,000 cells/well in 50 μL in Costar clear bottom white walled plates. In a separate plate, 25 μL of serially diluted antibodies at 4X concentration were added to wells containing 25 μL of either 25,000 cells of human or mouse $\alpha\beta x$ cells. After a brief mixing, the 50 μL mixture was transferred to the TMLE cell plates for a total volume of 100 μL and incubated at 37 °C for 16 h. 100 μL of ONE-Glo kit (#PRE6120) was added to each well and read after 3–5 min on the Envision plate reader.

αSMA imaging. Primary cells (passage 3–5) were grown on Cell carrier Ultra, col1 coated 96-well plates (Perkin Elmer, #6055700) at a density of 25,000 cells/well. Once the cells adhere, they were starved in serum free media for 24 h followed by addition of treatments i.e. 5 ng/mL TGF β (Biolegend #580702) \pm inhibitors. Cells were pre-treated with inhibitors for 30 min prior to the addition of TGF β stimulation. 48 hours post treatment, the cells were fixed in 4% methanol free paraformaldehyde (ThermoFisher Scientific #28908) for 20 min at room temperature and incubated with anti-alpha smooth muscle Actin antibody (Abcam #ab7817) at 1:4000 overnight at 4 °C. Following primary Ab incubation, cells were incubated with Goat anti-mouse secondary antibody (ThermoFisher Scientific #A32723) at 1:500 and Hoechst (ThermoFisher Scientific #62249) at 1:1000 for 1 h at

room temperature. The fixed and stained cells were imaged for immunofluorescence on Perkin Elmer's Opera Phenix high content Imager.

Mouse bleomycin lung fibrosis models. Adult male C57BL/6 mice (Taconic, Rensselaer, NY) were housed in a temperature and humidity-controlled facility with a 12 h light: 12-h dark cycle. Animals had ad libitum access to food (Purina Rodent Chow 5053, LabDiet, St. Louis, MO) and water. All procedures utilizing experimental animals were conducted in accordance with the Guide for the Care and Use of Laboratory Animals, and experimental procedures were reviewed and approved by the Institutional Animal Care and Use Committee at MRL, Kenilworth, NJ.

For osmotic minipump implantation, TFA salt of MK-0429 was formulated in 50% DMSO/50% H₂O at a concentration of 416 mg/mL. MK-0429 or vehicle solution were filled in minipumps (Alzet, # 1007D, flow rate 0.5 μ L/h). Minipumps were placed in mice subcutaneously in a pocket on the back between the shoulder blades. A small incision was made and a subcutaneous pocket formed by blunt dissection. A sterile minipump was inserted into the subcutaneous pocket. The incision was closed with staples or non-absorbable suture or absorbable (subcuticular) suture. The minipumps were used for continuous drug delivery for 2 weeks.

Mice at 12–13 weeks of age were randomized to 5 groups: saline, bleomycin instillation with vehicle (osmotic minipump), bleomycin instillation with MK-0429 treatment, bleomycin instillation with vehicle oral treatment, and bleomycin instillation with Nintedanib treatment. All mice were anaesthetized with isoflurane. Bleomycin was dosed by intra-tracheal (i.t) instillation in a volume of 50 μ L, at a dose of 1 unit/kg body weight. After instillation, mice were kept in a heads-up position for 2–5 min before putting into cages. MK-0429 (200 mg/kg) was administered by Osmotic pump from day 5 to day 14 and Nintedanib (60 mg/kg) was administered, p.o., q.d., for 14 days. Vehicle was dosed orally at 10 am daily from the day 5 to the end of the studies and dosing volume was 10 mL/kg. For plasma PK analysis, an aliquot of 50 μ L plasma was spiked into a 96-well plate, and 200 μ L of acetonitrile containing internal standard were added for protein precipitation. The mixture was vortexed, centrifuged at 4000 rpm for 20 min. 50 μ L of supernatant were mixed with 200 μ L H₂O and the final solution were injected for LC–MS/MS analysis. The methods for quantitative analysis were developed on UPLC (Waters) chromatographic system equipped with an API4000 QTrap mass spectrometer (Applied Biosystems, Concord, Ontario, Canada). Analyst 1.5 software packages (Applied Biosystems) were used to control the LC–MS/MS system and data acquisition and processing.

Histopathology analysis. Upon completion of the study, animals were euthanized and tissues were collected for histological assessment. Lung tissues were perfused with 10% formalin, fixed for 24 h, and then paraffin embedded. Tissue sections were stained with hematoxylin & eosin (H&E) and Masson's trichrome, subsequently evaluated under light microscope. The severity of histopathologic changes and fibrosis in the lung were graded as described previously by pathologists^{51,52}. Following deparaffinization and rehydration, each lung tissue section was processed to identify α SMA deposition by immunohistochemistry. The primary antibodies used were α SMA antibody from Sigma. The Aperio ScanScope XT Slide Scanner (Aperio Technologies) system was used to capture whole slide digital images with a 20 \times objective. Digital images were managed using Aperio Spectrum. The positive stains were identified and quantified using a macro created from a color deconvolution algorithm (Aperio Technologies). Statistical analysis was performed by using One-way ANOVA followed by Tukey's test.

Integrin co-immunoprecipitation and western blot analyses. Cells or lung tissue were lysed with assay buffer (50 mM Tris, pH7.4, 150 mM NaCl, 1 mM EDTA, 10% glycerol, 2% NP-40) with the addition of protease inhibitor (Roche cOMplete mini-pellet, EDTA free, #4693159001) and phosphatase inhibitor cocktails (Sigma #P5726). The total protein concentration was determined by Bradford reagent (Bio-Rad #5000006). 1 mg of cell lysates were incubated with anti- α v antibody (Enzo #ALX-803-304-C100) and Protein G magnetic beads (Pierce #88802) at 4 $^{\circ}$ C overnight. After washes, the beads were treated with 0.1X sample buffer with fluorescent dye and boiled at 95 $^{\circ}$ C for 5 min. The supernatant was subsequently subjected for Sally Sue Simple Western analysis from ProteinSimple²². The antibodies used for detecting integrin isoforms were shown in Supplemental Table S2, and anti-FAK and GAPDH antibodies were from Cell Signaling Transduction.

Molecular modeling. To generate a model for our antibodies, we employed the Antibody Modeler tool within MOE 2019 (Chemical Computing Group, Montreal, Canada) using the determined sequence for Ab-31 and related antibodies to generate a final Fab model. Default settings in MOE 2019 were used during model generation, with the highest scoring model of the ten produced models selected for further study.

To model how our antibodies may bind to integrin, previously published structures of α 5 β 1 integrin (PDB: 3VI4) and α v β 3 (PDB: 6AVQ) were used as models for antibody binding to integrin^{39,53}. Each structure was first prepared by deleting additional copies of integrin in the original crystal structures, followed by running the Structure Preparation and Protonate 3D tools within MOE 2019 to add missing side chains, loops, hydrogens, and cap termini using the Amber14EHT force field. Protein–Protein docking was then carried out in MOE 2019 using integrin as the receptor and the modeled antibody Fv region as the ligand while enabling both hydrophobic patch potentials and restraining the ligand site to the CDRs of the modeled Ab-31 structure as annotated by MOE 2019. The resulting poses were then visualized across Ab-31 and related antibodies which were also modeled, as well as across two distinct integrin structures to identify poses that were consistent with the previously described experimental data. The final model was then compared the published integrin-antibody complexes of Abituzumab (PDB: 4O02) and LM609 (PDB: 6AVQ)^{41,45}. All images were generated in MOE 2019.

Data availability

All data generated or analyzed during this study are included in this manuscript and its supplementary information files.

Received: 3 June 2020; Accepted: 5 January 2021

Published online: 22 January 2021

References

- Wilson, K. C. & Raghu, G. The 2015 guidelines for idiopathic pulmonary fibrosis: An important chapter in the evolution of the management of patients with IPF. *Eur. Respir. J.* **46**, 883–886. <https://doi.org/10.1183/13993003.01335-2015> (2015).
- Hynes, R. O. Integrins: Bidirectional, allosteric signaling machines. *Cell* **110**, 673–687. [https://doi.org/10.1016/s0092-8674\(02\)00971-6](https://doi.org/10.1016/s0092-8674(02)00971-6) (2002).
- Munger, J. S. *et al.* The integrin alpha v beta 6 binds and activates latent TGF beta 1: A mechanism for regulating pulmonary inflammation and fibrosis. *Cell* **96**, 319–328. [https://doi.org/10.1016/s0092-8674\(00\)80545-0](https://doi.org/10.1016/s0092-8674(00)80545-0) (1999).
- Kitamura, H. *et al.* Mouse and human lung fibroblasts regulate dendritic cell trafficking, airway inflammation, and fibrosis through integrin alphavbeta8-mediated activation of TGF-beta. *J. Clin. Invest.* **121**, 2863–2875. <https://doi.org/10.1172/JCI45589> (2011).
- Reed, N. I. *et al.* The alphavbeta1 integrin plays a critical in vivo role in tissue fibrosis. *Sci. Transl. Med.* **7**, 288. <https://doi.org/10.1126/scitranslmed.aaa5094> (2015).
- Henderson, N. C. *et al.* Targeting of alphav integrin identifies a core molecular pathway that regulates fibrosis in several organs. *Nat. Med.* **19**, 1617–1624. <https://doi.org/10.1038/nm.3282> (2013).
- Akhurst, R. J. & Hata, A. Targeting the TGFbeta signalling pathway in disease. *Nat. Rev. Drug. Discov.* **11**, 790–811. <https://doi.org/10.1038/nrd3810> (2012).
- Dong, X., Hudson, N. E., Lu, C. & Springer, T. A. Structural determinants of integrin beta-subunit specificity for latent TGF-beta. *Nat. Struct. Mol. Biol.* **21**, 1091–1096. <https://doi.org/10.1038/nsmb.2905> (2014).
- Horan, G. S. *et al.* Partial inhibition of integrin alpha(v)beta6 prevents pulmonary fibrosis without exacerbating inflammation. *Am. J. Respir. Crit. Care. Med.* **177**, 56–65. <https://doi.org/10.1164/rccm.200706-805OC> (2008).
- Maden, C. H. *et al.* Safety, tolerability and pharmacokinetics of GSK3008348, a novel integrin alphavbeta6 inhibitor, in healthy participants. *Eur. J. Clin. Pharmacol.* **74**, 701–709. <https://doi.org/10.1007/s00228-018-2435-3> (2018).
- Mu, D. *et al.* The integrin alpha(v)beta8 mediates epithelial homeostasis through MT1-MMP-dependent activation of TGF-beta1. *J. Cell. Biol.* **157**, 493–507. <https://doi.org/10.1083/jcb.200109100> (2002).
- Minagawa, S. *et al.* Selective targeting of TGF-beta activation to treat fibroinflammatory airway disease. *Sci. Transl. Med.* **6**, 241–279. <https://doi.org/10.1126/scitranslmed.3008074> (2014).
- Shrine, N. *et al.* New genetic signals for lung function highlight pathways and chronic obstructive pulmonary disease associations across multiple ancestries. *Nat. Genet.* **51**, 481–493. <https://doi.org/10.1038/s41588-018-0321-7> (2019).
- Hartman, G. D. *et al.* Non-peptide fibrinogen receptor antagonists. 1. Discovery and design of exosite inhibitors. *J. Med. Chem.* **35**, 4640–4642. <https://doi.org/10.1021/jm00102a020> (1992).
- Topol, E. J. *et al.* Comparison of two platelet glycoprotein IIb/IIIa inhibitors, tirofiban and abciximab, for the prevention of ischemic events with percutaneous coronary revascularization. *N. Engl. J. Med.* **344**, 1888–1894. <https://doi.org/10.1056/NEJM200106213442502> (2001).
- Murphy, M. G. *et al.* Effect of L-000845704, an alphaVbeta3 integrin antagonist, on markers of bone turnover and bone mineral density in postmenopausal osteoporotic women. *J. Clin. Endocrinol. Metab.* **90**, 2022–2028. <https://doi.org/10.1210/jc.2004-2126> (2005).
- Hutchinson, J. H. *et al.* Nonpeptide alphavbeta3 antagonists. 8. In vitro and in vivo evaluation of a potent alphavbeta3 antagonist for the prevention and treatment of osteoporosis. *J. Med. Chem.* **46**, 4790–4798. <https://doi.org/10.1021/jm030306r> (2003).
- Coleman, P. J. *et al.* Nonpeptide alphavbeta3 antagonists. Part 11: discovery and preclinical evaluation of potent alphavbeta3 antagonists for the prevention and treatment of osteoporosis. *J. Med. Chem.* **47**, 4829–4837. <https://doi.org/10.1021/jm049874c> (2004).
- Zhou, X. *et al.* An integrin antagonist (MK-0429) decreases proteinuria and renal fibrosis in the ZSF1 rat diabetic nephropathy model. *Pharmacol. Res. Perspect.* <https://doi.org/10.1002/prp2.354> (2017).
- Hahm, K. *et al.* Alphav beta6 integrin regulates renal fibrosis and inflammation in Alport mouse. *Am. J. Pathol.* **170**, 110–125. <https://doi.org/10.2353/ajpath.2007.060158> (2007).
- Moore, B. B. *et al.* Animal models of fibrotic lung disease. *Am. J. Respir. Cell. Mol. Biol.* **49**, 167–179. <https://doi.org/10.1165/rcmb.2013-0094TR> (2013).
- Harris, V. M. Protein detection by Simple Western™ analysis. *Methods Mol. Biol.* **1312**, 465–468. https://doi.org/10.1007/978-1-4939-2694-7_47 (2015).
- Ozawa, A. *et al.* Molecular basis of the ligand binding specificity of alphavbeta8 integrin. *J. Biol. Chem.* **291**, 11551–11565. <https://doi.org/10.1074/jbc.M116.719138> (2016).
- Weinreb, P. H. *et al.* Function-blocking integrin alphavbeta6 monoclonal antibodies: distinct ligand-mimetic and nonligand-mimetic classes. *J. Biol. Chem.* **279**, 17875–17887. <https://doi.org/10.1074/jbc.M312103200> (2004).
- Vogel, B. E. *et al.* A novel integrin specificity exemplified by binding of the alpha v beta 5 integrin to the basic domain of the HIV Tat protein and vitronectin. *J. Cell Biol.* **121**, 461–468. <https://doi.org/10.1083/jcb.121.2.461> (1993).
- Wu, C., Bauer, J. S., Juliano, R. L. & McDonald, J. A. The alpha 5 beta 1 integrin fibronectin receptor, but not the alpha 5 cytoplasmic domain, functions in an early and essential step in fibronectin matrix assembly. *J. Biol. Chem.* **268**, 21883–21888 (1993).
- Hall, E. R., Bibby, L. I. & Slack, R. J. Characterisation of a novel, high affinity and selective alphavbeta6 integrin RGD-mimetic radioligand. *Biochem. Pharmacol.* **117**, 88–96. <https://doi.org/10.1016/j.bcp.2016.08.003> (2016).
- Zhang, Z. *et al.* The alpha v beta 1 integrin functions as a fibronectin receptor but does not support fibronectin matrix assembly and cell migration on fibronectin. *J. Cell Biol.* **122**, 235–242. <https://doi.org/10.1083/jcb.122.1.235> (1993).
- Mazzieri, R., Munger, J. S. & Rifkin, D. B. Measurement of active TGF-beta generated by cultured cells. *Methods Mol. Biol.* **142**, 13–27. <https://doi.org/10.1385/1-59259-053-5:13> (2000).
- Hua, X., Miller, Z. A., Wu, G., Shi, Y. & Lodish, H. F. Specificity in transforming growth factor beta-induced transcription of the plasminogen activator inhibitor-1 gene: Interactions of promoter DNA, transcription factor muE3, and Smad proteins. *Proc. Natl. Acad. Sci. USA* **96**, 13130–13135 (1999).
- Yingling, J. M. *et al.* Tumor suppressor Smad4 is a transforming growth factor beta-inducible DNA binding protein. *Mol. Cell Biol.* **17**, 7019–7028 (1997).
- Campbell, M. G. *et al.* Cryo-EM reveals integrin-mediated TGF-beta activation without release from latent TGF-beta. *Cell* **180**, 490–501. <https://doi.org/10.1016/j.cell.2019.12.030> (2020).
- Lygoe, K. A., Norman, J. T., Marshall, J. F. & Lewis, M. P. AlphaV integrins play an important role in myofibroblast differentiation. *Wound Repair Regen.* **12**, 461–470. <https://doi.org/10.1111/j.1067-1927.2004.12402.x> (2004).

34. Grygielko, E. T. *et al.* Inhibition of gene markers of fibrosis with a novel inhibitor of transforming growth factor-beta type I receptor kinase in puromycin-induced nephritis. *J. Pharmacol. Exp. Ther.* **313**, 943–951. <https://doi.org/10.1124/jpet.104.082099> (2005).
35. Byron, A. *et al.* Anti-integrin monoclonal antibodies. *J. Cell Sci.* **122**, 4009–4011. <https://doi.org/10.1242/jcs.056770> (2009).
36. Humphries, J. D. *et al.* Dual functionality of the anti-beta1 integrin antibody, 12G10, exemplifies agonistic signalling from the ligand binding pocket of integrin adhesion receptors. *J. Biol. Chem.* **280**, 10234–10243. <https://doi.org/10.1074/jbc.M411102200> (2005).
37. Mould, A. P., Garratt, A. N., Askari, J. A., Akiyama, S. K. & Humphries, M. J. Identification of a novel anti-integrin monoclonal antibody that recognises a ligand-induced binding site epitope on the beta 1 subunit. *FEBS Lett.* **363**, 118–122. [https://doi.org/10.1016/0014-5793\(95\)00301-o](https://doi.org/10.1016/0014-5793(95)00301-o) (1995).
38. Lenter, M. *et al.* A monoclonal antibody against an activation epitope on mouse integrin chain beta 1 blocks adhesion of lymphocytes to the endothelial integrin alpha 6 beta 1. *Proc. Natl. Acad. Sci. USA* **90**, 9051–9055. <https://doi.org/10.1073/pnas.90.19.9051> (1993).
39. Xiong, J. P. *et al.* Crystal structure of the extracellular segment of integrin alpha Vbeta3. *Science* **294**, 339–345. <https://doi.org/10.1126/science.1064535> (2001).
40. Elez, E. *et al.* Abituzumab combined with cetuximab plus irinotecan versus cetuximab plus irinotecan alone for patients with KRAS wild-type metastatic colorectal cancer: the randomised phase I/II POSEIDON trial. *Ann. Oncol.* **26**, 132–140. <https://doi.org/10.1093/annonc/mdu474> (2015).
41. Mahalingam, B. *et al.* Atomic basis for the species-specific inhibition of alphaV integrins by monoclonal antibody 17E6 is revealed by the crystal structure of alphaVbeta3 ectodomain-17E6 Fab complex. *J. Biol. Chem.* **289**, 13801–13809. <https://doi.org/10.1074/jbc.M113.546929> (2014).
42. Wu, H. *et al.* Stepwise in vitro affinity maturation of Vitaxin, an alphav beta3-specific humanized mAb. *Proc. Natl. Acad. Sci. USA* **95**, 6037–6042. <https://doi.org/10.1073/pnas.95.11.6037> (1998).
43. Guthel, J. C. *et al.* Targeted antiangiogenic therapy for cancer using Vitaxin: A humanized monoclonal antibody to the integrin alphavbeta3. *Clin. Cancer Res.* **6**, 3056–3061 (2000).
44. Veeravagu, A. *et al.* Integrin alphavbeta3-targeted radioimmunotherapy of glioblastoma multiforme. *Clin. Cancer Res.* **14**, 7330–7339. <https://doi.org/10.1158/1078-0432.CCR-08-0797> (2008).
45. Borst, A. J. *et al.* The therapeutic antibody LM609 selectively inhibits ligand binding to human alphavbeta3 integrin via steric hindrance. *Structure* **25**, 1732–1739. <https://doi.org/10.1016/j.str.2017.09.007> (2017).
46. Takeda, Y., Tsujino, K., Kijima, T. & Kumanogoh, A. Efficacy and safety of pirfenidone for idiopathic pulmonary fibrosis. *Patient Prefer. Adherence* **8**, 361–370. <https://doi.org/10.2147/PPA.S37233> (2014).
47. Wollin, L. *et al.* Mode of action of nintedanib in the treatment of idiopathic pulmonary fibrosis. *Eur. Respir. J.* **45**, 1434–1445. <https://doi.org/10.1183/09031936.00174914> (2015).
48. Henderson, N. C. & Sheppard, D. Integrin-mediated regulation of TGFbeta in fibrosis. *Biochim. Biophys. Acta* **891–896**, 2013. <https://doi.org/10.1016/j.bbdis.2012.10.005> (1832).
49. Rosenthal, M. A. *et al.* Evaluation of the safety, pharmacokinetics and treatment effects of an alpha(nu)beta(3) integrin inhibitor on bone turnover and disease activity in men with hormone-refractory prostate cancer and bone metastases. *Asia Pac. J. Clin. Oncol.* **6**, 42–48. <https://doi.org/10.1111/j.1743-7563.2009.01266.x> (2010).
50. Sivasubramanian, A. *et al.* Broad epitope coverage of a human in vitro antibody library. *MAbs* **9**, 29–42. <https://doi.org/10.1080/19420862.2016.1246096> (2017).
51. Ashcroft, T., Simpson, J. M. & Timbrell, V. Simple method of estimating severity of pulmonary fibrosis on a numerical scale. *J. Clin. Pathol.* **41**, 467–470. <https://doi.org/10.1136/jcp.41.4.467> (1988).
52. Hubner, R. H. *et al.* Standardized quantification of pulmonary fibrosis in histological samples. *Biotechniques* **44**(507–511), 514–607. <https://doi.org/10.2144/000112729> (2008).
53. Nagae, M. *et al.* Crystal structure of alpha5beta1 integrin ectodomain: atomic details of the fibronectin receptor. *J. Cell Biol.* **197**, 131–140. <https://doi.org/10.1083/jcb.201111077> (2012).

Acknowledgements

The authors thank Zubia Naji for project management support and thank Xiaolan Shen, Audrey Chu, Dana Nojima, Mohammad Tabrizifard, Maarten Hoek, John Hunter, Ednan Bajwa, Paul Coleman, and Gordon Wollenberg for their valuable feedback throughout the work. We thank Dr. Jesse Nussbaum for his critical review of the manuscript. We thank Drs. Roy Zent and Ambra Pozzi at the Vanderbilt University for their valuable feedback. We thank Dr. Daniel Rifkin at New York University for his expertise and providing mink lung epithelial cells for latent TGFβ assays. Histological staining was provided by HistoBridge via Science Exchange. We acknowledge the dedicated assay development work of the late Mrs. Kim O'Neill while fighting late-stage cancer.

Author contributions

J.Z., M.G.-C., J.H., T.-Q.C., T.A., S.P., J.C.M., Z.R., H.H.S., and M.H. conceived the experiments; J.Z., T.W., A.S., J.J., J.M., S.T., M.J.E., W.M., K.O., D.G.L, T.H., Q.Z., and W.D. performed experiments; E.C.-J. and T.-Q.C. coordinated in vivo studies; S.A.H. and A.C.C. performed antibody structural modeling; J.Z., A.S., J.J., J.M., S.T., S.A.H., M.J.E., E.C.-J., H.Y.M., A.C.C., J.C.M., H.H.S., and M.H. wrote the manuscript; T.G., and S.T. provided critical expertise and feedback.

Competing interests

The authors (J.Z., T.W., A.S., J.J., J.M., S.T., S.A.H., M.J.E., W.M., K.O., M.G.-C., E.C.-J., D.G.L, T.H., Q.Z., W.D., H.Y.M., J.H., T.-Q.C., T.A., S.P., A.C.C., T.G., J.C.M., Z.R., S.T., H.H.S., M.H.) are/were employees of Merck Sharp & Dohme Corp., a subsidiary of Merck & Co., Inc., Kenilworth, NJ, USA and/or shareholders of Merck & Co., Inc., Kenilworth, NJ, USA.

Additional information

Supplementary Information The online version contains supplementary material available at <https://doi.org/10.1038/s41598-021-81253-0>.

Correspondence and requests for materials should be addressed to J.Z. or M.H.

Reprints and permissions information is available at www.nature.com/reprints.

Publisher's note Springer Nature remains neutral with regard to jurisdictional claims in published maps and institutional affiliations.



Open Access This article is licensed under a Creative Commons Attribution 4.0 International License, which permits use, sharing, adaptation, distribution and reproduction in any medium or format, as long as you give appropriate credit to the original author(s) and the source, provide a link to the Creative Commons licence, and indicate if changes were made. The images or other third party material in this article are included in the article's Creative Commons licence, unless indicated otherwise in a credit line to the material. If material is not included in the article's Creative Commons licence and your intended use is not permitted by statutory regulation or exceeds the permitted use, you will need to obtain permission directly from the copyright holder. To view a copy of this licence, visit <http://creativecommons.org/licenses/by/4.0/>.

© The Author(s) 2021